Temperature mapping near plasmonic nanostructures using fluorescence polarization anisotropy

G. Baffou[1], M. P. Kreuzer[1], F. Kulzer[1], and R. Quidant[1,2]

1 – ICFO – Institut de Ciencies Fotoniques, 08860 Castelldefels (Barcelona), Spain

2 – ICREA – Institució Catalana de Recerca i Estudis Avançats

guillaume.baffou@icfo.es

romain.quidant@icfo.es

Abstract: We report on a thermal imaging technique based on fluorescence polarization anisotropy measurements, which enables mapping the local temperature near nanometer-sized heat sources with 300 nm spatial resolution and a typical accuracy of 0.1 °C. The principle is demonstrated by mapping the temperature landscape around plasmonic nano-structures heated by near-infrared light. By assessing directly the molecules' Brownian dynamics, it is shown that fluorescence polarization anisotropy is a robust and reliable method which overcomes the limitations of previous thermal imaging techniques. It opens new perspectives in medicine, nanoelectronics and nanofluidics where a control of temperature of a few degrees at the nanoscale is required.

OCIS codes: (120.6810) Thermal effects; (180.2520) Fluorescence microscopy; (250.5403) Plasmonics

References and links

1. A. M. Gobin, M. H. Lee, N. J. Halas, W. D. James, R. A. Drezek, and J. L. West, "Near-Infrared Resonant Nanoshells for Combined Optical Imaging and Photothermal Cancer Therapy," Nano Lett. **7**, 1929–1934 (2007).
2. P. K. Jain, I. H. El-Sayed, and M. A. El-Sayed, "Au nanoparticles target cancer," Nano Today **2**, 18 (2007).
3. D. Pissuwana, S. M. Valenzuelaa, and M. B. Cortie, "Therapeutic possibilities of plasmonically heated gold nanoparticles," Trends Biotechnol. **24**, 62 (2006).
4. G. Han, P. Ghosh, M. De, and V. M. Rotello, "Drug and Gene Delivery using Gold Nanoparticles," NanoBioTechnology **3**, 40 (2007).
5. A. G. Skirtach, C. Dejugnat, D. Braun, A. S. Susha, A. L. Rogach, W. J. Parak, H. Möhwald, and G. B. Sukhorukov, "The Role of Metal Nanoparticles in Remote Release of Encapsulated Materials," Nano Lett. **5**, 1371 (2005).
6. L. Cao, D. Barsic, A. Guichard, and M. Brongersma, "Plasmon-assisted local temperature control to pattern individual semiconductor nanowires and carbon nanotubes," Nano Lett. **7**, 3523–3527 (2007).
7. G. L. Liu, J. Kim, L. Y., and L. P. Pee, "Optofluidic control using photothermal nanoparticles," Nat. Mater. **5**, 27 (2006).
8. D. Ross, M. Gaitan, and L. E. Locascio, "Temperature Measurement in Microfluidic Systems Using a Temperature-Dependent Fluorescent Dye," Anal. Chem. **73**, 4117 (2001).
9. M. Righini, A. S. Zelenina, C. Girard, and R. Quidant, "Parallel and selective trapping in a patterned plasmonic landscape," Nat. Phys. **3**, 477 (2007).
10. V. Garces-Chavez, R. Quidant, P. J. Reece, G. Badenes, L. Torner, and K. Dholakia, "Extended organization of colloidal microparticles by surface plasmon polariton excitation," Phys. Rev. B **73**, 085417 (pages 5) (2006).
11. A. Bar-Cohen, P. Wang, and E. Rahim, "Thermal management of high heat flux nanoelectronic chips," Microgravity Sci. Technol. **19**, 48 (2007).

#105458 - $15.00 USD Received 17 Dec 2008; revised 30 Jan 2009; accepted 30 Jan 2009; published 17 Feb 2009

12. D. Boyer, P. Tamarat, A. Maali, and B. Lounis, M. Orrit, "Photothermal Imaging of Nanometer-Sized Metal Particles Among Scatterers," Science **297**, 1160 (2002).
13. M. A. van Dijk, A. L. Tchebotareva, M. Orrit, M. Lippitz, S. Berciaud, D. Lasne, L. Cognet, and B. Lounis, "Absorption and scattering microscopy of single metal nanoparticles," Phys. Chem. Chem. Phys. **8**, 3486 (2006).
14. D. Lasne, G. A. Blab, S. Berciaud, M. Heine, L. Groc, D. Choquet, L. Cognet, and B. Lounis, "Single NanoParticle Photothermal Tracking (SNaPT) of 5 nm gold beads in live cells," Biophys. J. **91**, 4598 (2006).
15. H. M. Pollock and A. Hammiche, "Micro-thermal analysis: techniques and applications," J. Phys. D-Appl. Phys. **34**, R23 (2001).
16. J. W. Pomeroy, M. Kuball, D. J. Wallis, A. M. Keir, K. P. Hilton, R. S. Balmer, M. J. Uren, T. Martin, and P. J. Heard, "Thermal mapping of defects in AlGaN/GaN heterostructure field-effect transistors using micro-Raman spectroscopy," Appl. Phys. Lett. **87**, 103,508 (2005).
17. K. K. Liu, K. L. Davis, and M. D. Morris, "Raman spectroscopic measurement of spatial and temporal gradients in operating electrophoresis capillaries," Anal. Chem. **66**, 3744 (1994).
18. P. Löw, B. Kim, N. Takama, and C. Bergaud, "High-spatial-resolution surface-temperature mapping using fluorescent thermometry," Small **4**, 908 (2008).
19. G. A. Robinson, R. P. Lucht, and M. Laurendeau, "Two-color planar laser-induced fluorescence thermometry in aqueous solutions," Appl. Opt. **47**, 2852 (2008).
20. B. Samson, L. Aigouy, P. Löw, C. Bergaud, B. J. Kim, and M. Mortier, "ac thermal imaging of nanoheaters using a scanning fluorescent probe," Appl. Phys. Lett. **92**, 023,101 (2008).
21. B. Valeur, *Molecular Fluorescence: Principles and Applications* (Wiley-VCH, 2002). Chap. 5.
22. A. Kawski, "Fluorescence anisotropy: Theory and applications of rotational polarization," Crit. Rev. Anal. Chem. **23**, 459 (1993).
23. R. Zondervan, F. Kulzer, H. van der Meer, J. A. J. M. Disselhorst, and M. Orrit, "Laser-Driven Microsecond Temperature Cycles Analyzed by Fluorescence Polarization Microscopy," Biophys. J. **90**, 2958 (2006).
24. W. G., "Polarization of the fluorescence of macromolecules. 1. Theory and experiment method," Biochem J. **51**, 145 (1952).
25. A. H. A. Clayton, Q. S. Hanley, D. J. Arndt-Jovin, V. Subramaniam, and T. M. Jovin, "Dynamic fluorescence anisotropy imaging microscopy in the frequency domain (rFLIM)," Biophys. J. **83**, 1631–1649 (2002).
26. R. F. Chen and R. L. Bowman, "Fluorescence polarization - measurement with ultraviolet-polarizing filters in a spectrophotofluorometer," Science **147**(3659), 729–732 (1965).
27. N. Periasamy, M. Armijo, and A. S. Verkman, "Picosecond rotation of small polar fluorophores in the cytosol of sea-urchin eggs," Biochem. **30**, 11,836–11,841 (1991).
28. N. S. Cheng, "Formula for the viscosity of a glycerol-water mixture," Ind. Eng. Chem. Res. **47**, 3285 (2008).
29. D. Axelrod, "Carbocyanine dye orientation in red-cell membrane studied by microscopic fluorescence polarization," Biophys. J. **26**, 557–573 (1979).
30. F. X. Gu, R. Karnik, A. Z. Wang, F. Alexis, E. Levy-Nissenbaum, S. Hong, R. S. Langer, and O. C. Farokhzad, "Targeted nanoparticles for cancer therapy," Nano Today **2**, 14 (2007).
31. K. Maier-Hauff, R. Rothe, R. Scholz, U. Gneveckow, P. Wust, B. Thiesen, A. Freussner, A. von Deimling, N. Waldoefner, R. Felix, and A. Jordan, "Intracranial thermotherapy using magnetic nanoparticles combined with external beam radiotherapy: Results of a feasibility study on patients with glioblastoma multiforme," J. Neuro-Oncol. **81**, 53 (2007).
32. B. Nikoobakht and M. A. El-Sayed, "Preparation and growth mechanism of gold nanorods (NRs) using seed-mediated growth method," Chem. Mat. **15**, 1957 (2003).

Efforts to measure and control temperature at the nanoscale are no longer motivated only by fundamental interest, but are increasingly becoming important in many areas of nanotechnology including photothermal therapeutic medicine [1, 2, 3, 4, 5], nanoscale catalysis [6], nanofluidics [7, 8, 9, 10], micro and nanoelectronics [11] and photothermal imaging [12], spectroscopy [13] and nanoparticle tracking [14]. Along with the need of understanding thermal processes at the micro and nanoscale, several techniques aiming at high resolution temperature mapping have been proposed. Scanning Thermal Microscopy (SThM) uses a composite sharp tip to directly probe the temperature of the sample surface [15]. Although it allows a spatial resolution lower than 100 nm, this technique is only suited for surface science investigations and is known to remain slow and invasive. More recently, a collection of optical-based temperature probing techniques have been proposed based on the temperature dependence of either Raman spectra [16, 17], fluorescence intensity/spectra/time correlation [8, 18, 19, 20] or infrared spectra. However, none of these techniques combines the advantages of reliability, fast readout rate and high-resolution making them prohibitive for temperature imaging in Nanotechnology.

#105458 - $15.00 USD Received 17 Dec 2008; revised 30 Jan 2009; accepted 30 Jan 2009; published 17 Feb 2009

Here we report on an optical-based thermal imaging technique which consists in introducing fluorescent molecules inside the medium of interest and mapping the emitted fluorescence polarization anisotropy (FPA). The FPA is directly related to rotational diffusion induced by molecular Brownian dynamics [21, 22], which explains why this technique naturally achieves reliable temperature measurements. So far, FPA measurements have been mainly used in polymer science to determine molecular orientation or in biology to measure fluid microviscosity. One recent study utilized fluorescence polarization measurements to investigate temperature cycles and heating of an extended, unstructured chromium film in a cryogenic setting [23]. The underlying physics of FPA is well established. In general, a population of fluorophores illuminated by linearly polarized incident light re-emits partially polarized fluorescence due to the random orientation of the molecules [21, 22]. The polarization anisotropy r of the fluorescence is defined as:

$$r = \frac{I_{\parallel} - I_{\perp}}{I_{\parallel} + 2\,I_{\perp}} \tag{1}$$

where $I_{\parallel}$ and $I_{\perp}$ are the intensities of the fluorescence polarized parallel and perpendicular with respect to the incident polarization. This measurement is usually carried out in the so-called L-configuration with orthogonal excitation and detection paths [21, 24]. For randomly oriented fluorophores whose absorption and emission dipolar moments are parallel, the theoretical polarization anisotropy r_0 in absence of any molecular motion is maximum and reaches a value of 0.4. r_0 is called the *fundamental* or *limiting anisotropy*. The measured value of r is closely related to molecular rotation arising from Brownian dynamics according to Perrin's equation:

$$\frac{1}{r} = \frac{1}{r_0}\left(1 + \frac{\tau_{\mathrm{F}}}{\tau_{\mathrm{R}}}\right) \tag{2}$$

where τ_{R} is the rotational correlation time and τ_{F} the fluorescence life time. This equation means that substantial molecular rotation (induced by its Brownian dynamics) during the lifetime of the excited state leads to a fluorescence depolarization, i.e., a lower value of r. The key point of the technique is that an increase of the temperature contributes to lower the FPA r since it gives rise to a faster rotation of the molecules, i.e., a lower value of τ_{R}. This happens according to the Debye–Stokes–Einstein equation [21, 22]:

$$\tau_{\mathrm{R}} = \frac{V\,\eta(T)}{k_{\mathrm{B}}\,T} \tag{3}$$

where T is the temperature, $\eta(T)$ the dynamic viscosity of the medium, V the hydrodynamic molecular volume and k_{B} the Boltzmann constant. The maximum temperature sensitivity of r is achieved when τ_{R} is of the order of magnitude of the fluorescence lifetime τ_{F} (Eq. (2)). The sensitivity of the method can be enhanced if the fluid furthermore experiences substantial variations of its viscosity $\eta(T)$ within the temperature range of interest.

In the present experiment, we consider two kinds of gold nanostructures acting as nanometer-sized heat sources: lithographic nanowires and colloidal nanorods. In both cases, the nanostructures lie onto a glass substrate and are embedded in a 30 µm thick layer of a glycerol-water (4:1) mixture containing fluorescein molecules ($c = 1.4 \times 10^{-4}$M). A glass coverslip is placed on top of the solution layer to avoid water exchange with the surrounding air, which could affect the glycerol-water ratio and hence the fluid viscosity. The viscosity of glycerol decreases by more than one order of magnitude from 20 to 50 °C, which makes FPA measurements in glycerol highly temperature sensitive. Fluorescein is a xanthene-type chromophore (see inset Fig. 2), characterized by a high photostability and a fluorescence quantum efficiency close to 100%. Fluorescein in pure glycerol exhibits a rotational correlation time τ_{R} around 150 ns at 20 °C,

#105458 - $15.00 USD Received 17 Dec 2008; revised 30 Jan 2009; accepted 30 Jan 2009; published 17 Feb 2009

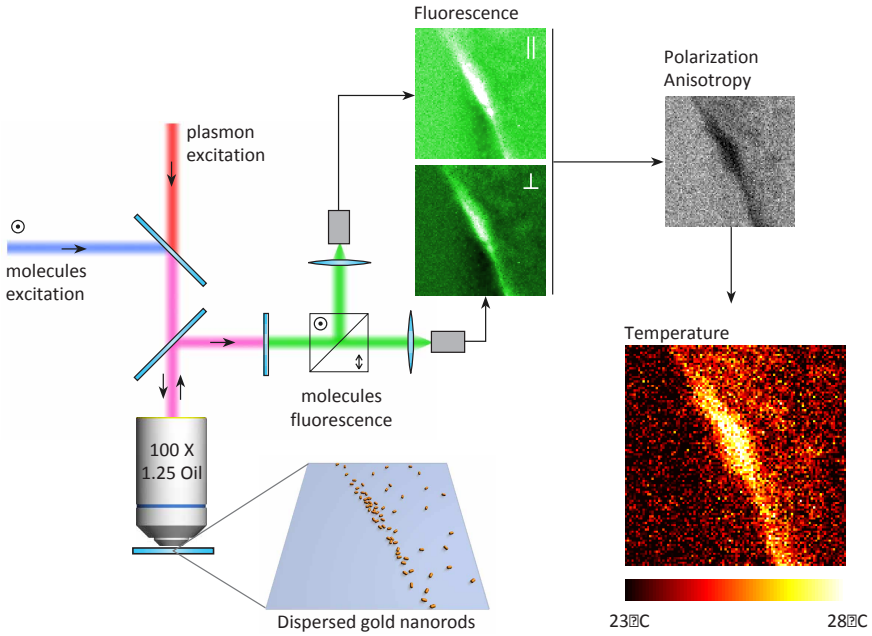

Fig. 1. Schematic of the experimental configuration and procedure. Two laser beams (for heating in the NIR and for probing at 473 nm) are overlapped prior to entering the objective of a confocal microscope. The sample is scanned through the focus to obtain an image. The collected fluorescence light is divided by a polarizing cube and sent to two avalanche photodiodes (APDs) measuring parallel and perpendicular polarizations. From these two maps, the FPA map is calculated using Eq. (1) and the temperature map is obtained using the calibration curve presented in Fig. 2. To illustrate the technique, a measurement on dispersed nanorods over a 30μm×30μm area is presented.

while its fluorescence life time τ_F is about 4 ns. Consequently, we use a glycerol-water (4:1) mixture to reduce the viscosity from 1400 to 60 mPa·s and the rotational correlation time to $\tau_R = 6$ ns. This results in a much stronger variation of the polarization anisotropy between 20 and 50 °C, our window of interest.

The experimental configuration and processing is sketched in Fig. 1. Using a confocal microscope, the fluorescein molecules are excited by a linearly polarized 473 nm laser beam while the parallel and orthogonal components of the collected fluorescence are separated by a polarizing cube and sent to two avalanche photodiodes (APDs). In all the experiments, the power applied for fluorescence excitation was around 0.1 μW right before the objective entrance. Heating of gold nanostructures is performed using a CW near-infrared (NIR) laser beam from a Ti:sapphire laser, coincident with the blue excitation light. To maximize the temperature increase due to absorption of the metal, the wavelength is tuned to the localized plasmon band of the nanostructures. Both the blue and the NIR beams are focused and overlapped on the sample through the objective of the confocal microscope (100 ×, NA 1.25) and scanned across the sample plane for simultaneous local heating and temperature measurement.

In order to extract the temperature from the FPA map, a previous calibration has to be done. Figure 2(a) plots the FPA measurements in the 4:1 glycerol-water mixture as a function of the temperature. This calibration curve was performed using a custom made fluorimeter directly mounted on the two APD detection part of the setup described above. This fluorimeter com-

#105458 - $15.00 USD Received 17 Dec 2008; revised 30 Jan 2009; accepted 30 Jan 2009; published 17 Feb 2009

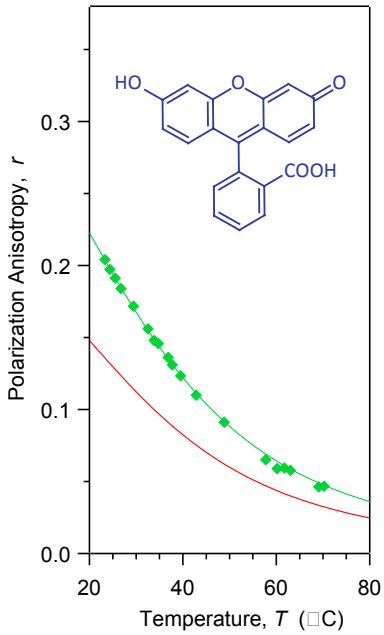

Fig. 2. Fluorescence polarization anisotropy calibration. Theoretical curve (solid green line) of fluorescence polarization anisotropy as a function of the temperature for fluorescein dissolved in a glycerol-water (4:1) mixture, showing a good agreement with the experimental measurements (green diamonds) along with the calculated corrected curve (red solid line) associated to our high-NA objective. The chemical structure of fluorescein is represented in the inset.

prises a resistor and a thermocouple enabling us to both vary and measure the temperature over the range of interest. The experimental data agree very well with the temperature-dependent polarization anisotropy of a glycerol-water mixture calculated using Eqs. (2) and (3) (solid line, Fig. 2(a)). The best fit is obtained for a glycerol mass fraction $C_m = 0.785 \pm 0.004$ which is fairly close to the intended value of 0.835. For the other parameters, and according to the literature, we used a fluorescence lifetime τ_F of 3.7 ns [25], a limiting anisotropy r_0 of 0.38 [26], a molecular hydrodynamic volume V of 0.41 nm^3 [27] and the empirical formula derived by Cheng [28] for the glycerol-water mixture viscosity. The calibration curve obtained from this data has to be adjusted for our subsequent microscopy measurements in order to account for the high numerical aperture of the objective and its intrinsic depolarization factor. The Axelrod method [29] is usually employed for this purpose in biology and polymer sciences. Figure 2(b) shows the corrected curve obtained for our Olympus objective (100×, NA 1.25) using this method.

In order to explain in detail the image acquisition and data processing, we first describe results obtained on single 250 nm wide and 30 nm thick gold nanowires prepared by conventional e-beam lithography combined with lift off. Figure 3 shows two sets of measurements, one without heating Figs. 3(b)-(e) and the other one while heating Figs. 3(f)-(i) with a 775 nm laser light linearly polarized perpendicularly to the nanowire axis. The scan proceeds upward, line by line and from left to right.

Figures 3(b) and (c) show the fluorescence intensity maps recorded without heating for both parallel $I_{\parallel}$ and perpendicular $I_{\perp}$ polarizations. Because it acts as a mirror and/or scatterer of

#105458 - $15.00 USD Received 17 Dec 2008; revised 30 Jan 2009; accepted 30 Jan 2009; published 17 Feb 2009

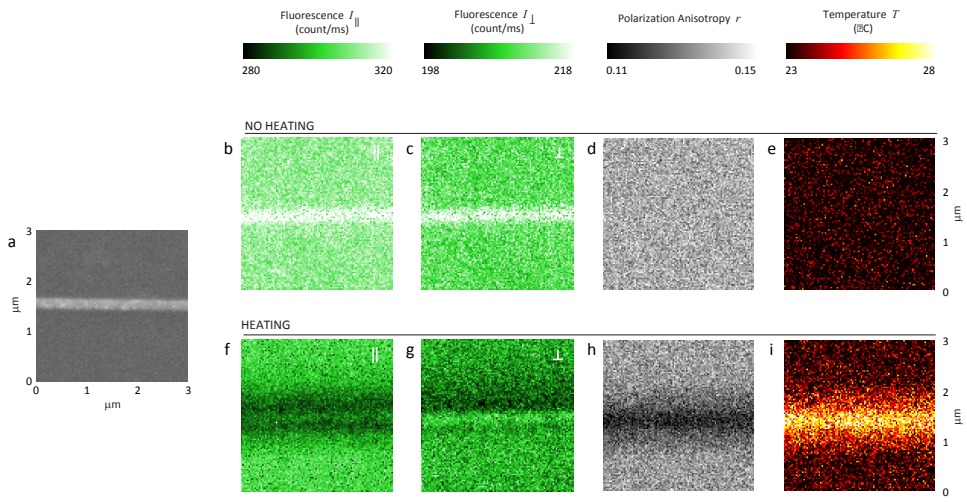

Fig. 3. (a), Scanning Electron Microscopy (SEM) image (3µm×3µm) of a 200 nm wide and 40 nm thick gold nanowire, corresponding to the area of interest. (b), (c), maps of the fluorescence intensities with parallel and perpendicular polarizations with respect to the incident light, no heating is performed in this first case. (d) fluorescence polarization anisotropy map calculated from images b and c using Eq. (1). (e) associated temperature distribution. (f), (g), maps of the fluorescence intensities with parallel and perpendicular polarizations while heating. (h), associated fluorescence polarization anisotropy map and (i) temperature distribution.

the fluorescence, the gold region appears brighter than the surroundings. These images also gives us the resolution of our confocal measurement which has been estimated to 300 nm. The associated FPA and the temperature maps (Figs. 3(d) and (e)) are perfectly uniform which is consistent with the fact that no heating of the nanowire is produced. Interestingly, r and T maps are not affected by the inherent non-uniformity of $I_{\parallel}$ and $I_{\perp}$ observed in Figs. 3(b) and (c). This differs from other fluorescence-based techniques where a normalization process is required. In our case, this feature illustrates how r is exclusively related to Brownian motion and does not depends on the total intensity (see Eq. (1)).

Figures 3(f) and (g) show the fluorescence intensity maps while heating with NIR light. Two effects are responsible for the contrast variation on these images: (i) due to the temperature increase, the depolarization effect tends to increase the orthogonal fluorescence intensity $I_{\perp}$ and decrease (twice as much) the parallel fluorescence intensity $I_{\parallel}$, (ii) the temperature increase is also responsible of an overall reduction of the fluorescence intensity associated to an increase of the molecular population in the dark state. However, since this latter side-effect affects equally both polarization intensities, this has no consequences on the FPA calculation (see Eq. (1)) and temperature measurement. Similarly, any unwanted fluorescence intensities variations resulting from e.g. mechanical noise, photobleaching or uncontrolled variation of the pump laser intensity, would not affect the temperature acquisition. Due to heating, a substantial decrease of the FPA along the wire is observed (Fig. 3(h)) which corresponds to an increase of the metal temperature (Fig. 3(i)) of a few degrees. In order to study the heating dynamics of the nanowire, a series of temperature measurements was performed as a function of the NIR laser power entering the objective. The results plotted in Fig. 4 verify that the temperature follows a linear dependency, as is expected for a linear absorption process. This remains true for a temperature

#105458 - $15.00 USD Received 17 Dec 2008; revised 30 Jan 2009; accepted 30 Jan 2009; published 17 Feb 2009

increase of about 10 °C, without hysteresis. At higher temperature, the system may eventually get modified, especially for very small structures, presumably due to temperature-induced fluid convection which tends to move the nanostructures a couple of micrometers away.

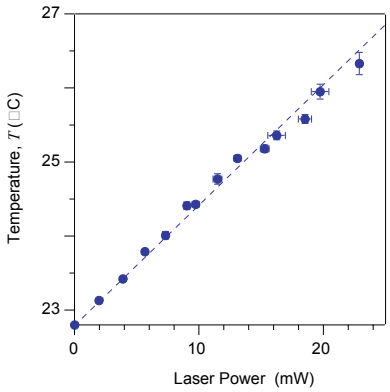

Fig. 4. Average temperature of the gold nanowire as a function of the power of the heating NIR light showing an expected linearity.

Photothermal cancer therapy and drug delivery based on gold nanoparticles are promising areas of research. Using passive or active targeting, it is now possible to effect the uptake of gold nanoparticles (spheres, nanoshells or nanorods) specifically into living cancer cells [30]. A subsequent NIR irradiation at the plasmonic resonance frequency can give rise to a local temperature increase of the nanoparticles damaging the cancer cells without affecting the healthy surrounding tissue. One of the major issues of all photothermal methods is to control local temperatures of $42-45$ °C (hyperthermia) or higher (thermoablation) within the entire tumor [31]. For this purpose, a very accurate monitoring of the temperature in required to ensure working in the desired regime. In this context, we used the FPA thermal imaging technique on an ensemble of colloidal nanorods (NR) as a model system which mimics the actual distribution obtained in cells. Gold NRs were synthesized by the seed mediated growth approach according to Nikoobakht et al. [32]. This procedure yielded rods with average dimensions of 50 nm $\times$ 12 nm (aspect ratio 4:1), whose extinction spectrum features a characteristic peak at 766 nm corresponding to the longitudinal plasmon mode. Subsequently excess molecular ligands (CTAB) were firstly filtered and then removed by numerous centrifugation cycles and replacing the supernatant with deionized water. A drop of the solution, 2 mm wide, was deposited on a glass sample and was allowed to evaporate slowly. This way large variations of NR deposits were observed, from well dispersed NRs in the center to agglomerated NRs along the drop circumference. The sample was covered with the same glycerol-water-fluorescein solution as previous and the heating laser wavelength was set at 770 nm to match the NR plasmon resonance. Figure 5(a) displays an optical image (recorded with a CCD camera) of the drop edge. For the FPA measurements, we chose an area showing large variations of gold NR concentrations in a single image, from agglomerated (dark areas) to more dispersed (bottom left area). The upper right part corresponds to the region outside of the drop. In Fig. 5(b), both fluorescence polarization maps are overlapped using a color convention where green and red correspond to parallel and orthogonal fluorescence polarizations, respectively. The associated temperature map is displayed in Fig. 5(c). No temperature variation is observed outside the drop edge (upper right part) as expected since no NRs are present in this region. Temperature contrasts are indeed only observed where the NRs are bound, with a more pronounced temperature increase where

#105458 - $15.00 USD Received 17 Dec 2008; revised 30 Jan 2009; accepted 30 Jan 2009; published 17 Feb 2009

the NR are agglomerated. In the bottom left corner of the image, a slight temperature increase can be measured, 23.8±0.1 °C, compared with the upper right corner which remained at room temperature: 23.1±0.1 °C. 0.1 °C is the typical temperature accuracy that can be reached using a 40 ms long exposure time per pixel. In a biological environment, the viscosity is likely to be much lower than our glycerol-water mixture making prohibitive the use of usual fluorescent molecules because of the too fast molecular brownian dynamics. However it remains possible to match the fluorescence life time and the rotational correlation time in aqueous medium by using fluorophores a few nanometers in size such as fluorescent proteins.

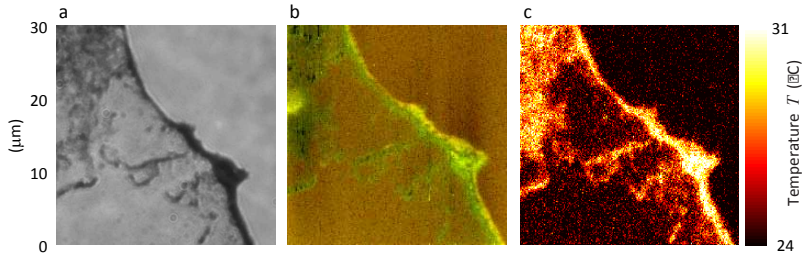

Fig. 5. Temperature mapping near dispersed gold nanorods. (a), Optical image (30μm×30 μm) of dispersed and agglomerated nanorods (NRs). (b), Fluorescence polarization anisotropy of the fluorescein molecules surrounding the gold nanorods and sensing the temperature variations. (c), Temperature map calculated from image (b).

In conclusion, we have introduced the use of fluorescence polarization anisotropy (FPA) to measure and map the temperature increase near nano-sized heat sources. The data demonstrate a typical temperature accuracy of a tenth of a degree and a spatial resolution of 300 nm. Because FPA is directly sensitive to fluorophore Brownian dynamics, it naturally provides a direct and reliable measurement of the actual local temperature. In particular, the method is non sensitive to side effects like photobleaching or thermal damage of the fluorophores. This feature makes the technique particularly robust and reliable. The applicability of the method has been successfully demonstrated on plasmonic gold nanostructures heated by coupling with NIR light to their plasmon resonance, but can be extended to any kind of heat source and geometry.

Acknowledgments

This research has been funded by the Spanish Ministry of Sciences through grants no. TEC2007-60186/MIC and no. CSD2007-046-NanoLight.es and by the fundació CELLEX. M. P. K. and F. K. acknowledge support from the *Ramón y Cajal* program.

#105458 - $15.00 USD Received 17 Dec 2008; revised 30 Jan 2009; accepted 30 Jan 2009; published 17 Feb 2009